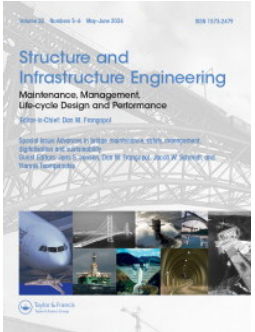

Taylor & Francis
Taylor & Francis Group

Structure and Infrastructure Engineering

Maintenance, Management, Life-Cycle Design and Performance

ISSN: 1573-2479 (Print) 1744-8980 (Online) Journal homepage: www.tandfonline.com/journals/nsie20

Collapse test of the Vecht Bridge: behaviour of post-tensioned concrete slab-between-girder bridges

Sebastiaan W. H. Ensink , Eva O. L. Lantsoght & Max A. H. Hendriks

To cite this article: Sebastiaan W. H. Ensink , Eva O. L. Lantsoght & Max A. H. Hendriks (2026) Collapse test of the Vecht Bridge: behaviour of post-tensioned concrete slab-between-girder bridges, Structure and Infrastructure Engineering, 22:5-6, 827-840, DOI: 10.1080/15732479.2025.2593589

To link to this article: https://doi.org/10.1080/15732479.2025.2593589

STRUCTURE AND INFRASTRUCTURE ENGINEERING
2026, VOL. 22, NOS. 5–6, 827–840
https://doi.org/10.1080/15732479.2025.2593589

Check for updates

Collapse test of the Vecht Bridge: behaviour of post-tensioned concrete slab-between-girder bridges

Sebastiaan W. H. Ensink[a], Eva O. L. Lantsoght[a,b] and Max A. H. Hendriks[a,c]

[a]Concrete Structures, Department of Engineering Structures, Civil Engineering and Geosciences, Delft University of Technology, Delft, The Netherlands; [b]Politécnico, Universidad San Francisco de Quito, Quito, Ecuador; [c]NTNU, Trondheim, Norway

ABSTRACT

In the Netherlands, approximately 70 prestressed slab-between-girder bridges are present, built between the 1950s and 1970s. These bridges typically do not fulfil the requirements for shear in an assessment, but show no signs of distress upon inspection. Additional load-carrying mechanisms and effects of global bridge behaviour, such as compressive membrane action, compressive arch action, load (re)distribution, and the influence of the crossbeams, which could significantly enhance the structural capacity, are typically not considered in the assessment calculations. This paper studies the global structural behaviour experimentally of the full slab-between-girder bridge system as compared to the isolated T-girder. For this purpose, two spans of an existing multi-span T-girder bridge, the Vecht Bridge, built in 1962 were tested. In total, three experiments were carried out in span 4 (full system), and four experiments in span 2 (after applying saw cuts in the deck to create isolated girders). This paper reviews the state-of-the-art regarding collapse testing, global bridge behaviour, and slab-between-girder bridges in the Netherlands. Then, the results of the experiments are presented and analysed. It is expected that these experimental results will form the basis of improved assessment methods for slab-between-girder bridges in the Netherlands and beyond.

ARTICLE HISTORY
Received 19 February 2025
Revised 8 April 2025
Accepted 17 June 2025

KEYWORDS
Bridge assessment; collapse test; flexure-shear; global bridge behaviour; numerical modelling; prestressed girders; shear-tension; system behaviour

1. Introduction

After the Second World War, the Dutch highway network was developed, resulting in the construction of a many bridges, including reinforced concrete slab bridges, prestressed girder bridges, and larger post-tensioned bridges, using either post-tensioned bulb-T girders or boxes. The bridges from that era are now reaching the end of their originally intended service life (Lantsoght et al., 2013) and their safety and adequacy are subject to discussion. Upon assessment, engineers are faced with live loads as prescribed by the currently governing code NEN-EN 1991-2:2003 (CEN, 2003) that are heavier than those used in the past and during the design stage. Moreover, on the capacity side of the equation, the shear capacity determined during design with the national codes from the past (Dutch Institute for Normalization, 1962) tends to be higher than the shear capacity obtained using the currently governing Eurocode NEN-EN 1992-1-1:2005 (CEN, 2005). In addition, for concrete girder bridges, the requirements for minimum shear reinforcement in the currently governing Eurocode NEN-EN 1992-1-1:2005 (CEN, 2005) will result in larger percentages of minimum stirrups than provided in past designs.

As a result, the assessment of existing concrete bridges in the Netherlands for shear is an important topic.

In the Netherlands, the post-tensioned bulb-T girder bridges used to be constructed with the slab cast between the top flanges of the girder, instead of cast on top of the top flanges. This system is then post-tensioned transversally, and crossbeams are used to generate global bridge behaviour. This system is known in France as 'viaduc à travées indépendantes à poutres pr écontraintes', abbreviated as 'VIPP'. Figure 1 shows the construction, using early principles of precasting, of the post-tensioned girder on site, and the transportation for construction. At the moment, about 70 of these bridges are still in service in the Netherlands. Upon initial assessment, the shear capacity of the slabs was considered governing. However, experimental research indicated that compressive membrane action develops in the slabs, so that the punching capacity is on average 2.32 times higher than when assessed using the punching shear provisions from the currently governing Eurocode NEN-EN 1992-1-1:2005 (CEN, 2005; Amir, 2014; Amir et al., 2016). Experimental research also addressed the question whether compressive membrane action acts under cycles of loading, and it was found indeed that the reduction of the capacity is in line with the reduction of concrete under cycles of compression (Lantsoght et al., 2019a; 2019b, 2019c). As a result of these insights, the focus of assessment shifted to the shear capacity of the prestressed girders, which now

CONTACT Eva O. L. Lantsoght elantsoght@usfq.edu.ec Diego de Robles y Pampite s/n, Campus Cumbaya, Universidad San Francisco de Quito, EC 170157 Quito, Ecuador.

Supplemental data for this article can be accessed online at https://doi.org/10.1080/15732479.2025.2593589.

(a) (b)

Figure 1. Construction of a slab-between-girder bridge (Van Brienenoord Bridge, Approach Bridge, Rotterdam 1963) (Rijkswaterstaat, 2020): (a) prefabrication of girder on site; (b) on-site transportation of prefabricated girder using railway track.

became critical for assessment of the bridge (Lantsoght et al., 2021; Zhang et al., 2020). In a number of cases, the girders are found to be shear-critical and insufficient upon assessment, but inspections indicate no signs of distress or cracking.

Aspects that are not considered in the assessment of the girders are related to load distribution, which differs in site conditions from the assumptions used in an assessment, and additional mechanisms and load paths that develop in the global bridge structure, which increase the ultimate capacity. For the bridge type studied, the following system effects were indicated as potentially occurring: compressive membrane action in the deck (even for cases when the concentrated load is not placed in the middle of the span of the slab; effect in the transverse direction), compressive arching action in the post-tensioned girder (effect in the longitudinal direction), differences in load distribution and redistribution between girders (effect in the transverse direction), and the intermediate support provided by the crossbeams (effect in the longitudinal direction).

This paper addresses the question of how global bridge mechanics and system behaviour increases the capacity of slab-between-girder bridges. To answer this question, we reviewed the literature on collapse testing and global bridge behaviour, carried out collapse tests on a bridge that was being decommissioned, and analysed the test results in the light of the system behaviour.

2. Literature review

2.1. Collapse testing

Bridge testing can be divided into diagnostic load testing, proof load testing, and collapse testing (Alampalli et al., 2021). The first two types of bridge tests are used for bridge assessment (Lantsoght, 2024; Pimentel et al., 2023; Saroufim et al., 2023), whereas the latter type is only used for research purposes. Collapse tests provide a unique opportunity to analyse the full load-carrying capacity and failure mechanisms in real bridge structures, with all relevant details and after years of service. At the same time, collapse tests involve very high magnitude loads, and pose a large risk during the execution. As such, collapse tests need to be very carefully prepared.

Table 1 gives an overview of relevant collapse tests that resulted in a failure in the girder in prestressed concrete girder bridges. This overview includes one frame structure, the Stora Höga 2 case. The information about these tested bridges is compiled from the literature review of collapse tests by Bagge et al. (Bagge et al., 2018), complemented with the information about the Chikubetsu bridge (Sato et al., 2019). The review by Bagge et al. (Bagge et al., 2018) included the information of 30 concrete bridges tested to failure, of which the majority were reinforced concrete slab or beam bridges, and only three prestressed concrete slab bridges and seven prestressed concrete girder bridges were identified. Table 1 includes information about the failure mode, using F for flexural failure, P for punching and S for shear, and the loading system, using W for kentledge weights applied directly to the bridge and HJ for hydraulic jacks. All bridges in Table 1 are roadway bridges, except for the South Bank bridge, which was a pedestrian bridge. The only bridge which consists of prestressed girders (T-beams in this case) and the slab cast between the girder top flanges is the Chikubetsu bridge. This bridge has only four girders in the cross-section and did not fail in shear.

From the collapse tests presented in Table 1, it can be concluded that there is technical value in testing the Vecht Bridge to fail in shear, as it presents a case that has not been tested before. In comparison to the Chikubetsu bridge, the Vecht bridge has a larger numbers of girders in the section (15 compared to 4) and the tests were designed to result in a shear failure rather than a flexural failure, as observed in the Chikubetsu bridge.

2.2. Global bridge behaviour

2.2.1. Live load distribution

In terms of global bridge behaviour, live load distribution is the most commonly addressed aspect during design. Here, it is important to distinguish load distribution, based on linear elastic bridge behaviour, to load redistribution, which occurs

Table 1. Prestressed girder bridges tested to failure (Ensink, 2024).

Name	Country	Construction year	Test year	Length [m]	Nr of spans	Failure mode	Loading system
South Bank	UK	1948	1952	86.56	4	F	W
Boiling Fork Creek	USA	1963	1970	80.47	4	P + S	HJ
Penn State University	USA	1977	1981	36.88	1	F	HJ
Stora Höga 2	Sweden	1980	1989	31.00	1	S	HJ
Seoul-Pusan	South Korea	1971	2000	360.00	12	F	HJ
Xin Xing Tang	China	1995	2005	114.00	3	F	W
Kiruna	Sweden	1959	2014	121.50	5	S + P-S	HJ
Chikubetsu	Japan	1960	2019	180.00	5	F	HJ

after cracking, when more load may be redistributed to adjacent girders. Live load distribution is typically based on simplified models: either using analytical methods such as those developed by Guyon and Massonnet (Bareš et al., 1968) or Engesser-Courbon (Benítez et al., 2022), using linear finite element models, or by using code-prescribed distribution factors. ACI 342 has provided guidance on how to derive flexural live load distribution factors from diagnostic load tests (ACI Committee 342, 2016).

Experimental evidence of the live load distribution for shear in post-tensioned T-girder bridges with cast-in-between slabs is limited, and is only obtained through diagnostic load tests, which do not provide insights on the post-cracking redistribution and distribution at the ultimate limit state. Experimental results from diagnostic load tests are available of slab-on-girder bridges (Arockiasamy & Amer, 1998; Idriss & Liang, 2010; Jáuregui & Barr, 2004; Mordak & Manko, 2008; Wekezer et al., 2004). In terms of code-prescribed distribution factors, we can highlight the live load distribution factors from AASHTO §4.6.2.2 (AASHTO, 2015) for shear. The AASHTO tables address both flexure and shear, and internal and external girders. The live load distribution factor (DF) for shear at an interior girder is prescribed as (using S as the spacing of the girders in [ft]):

$$DF = 0.36 + \frac{S}{25.0} \tag{1}$$

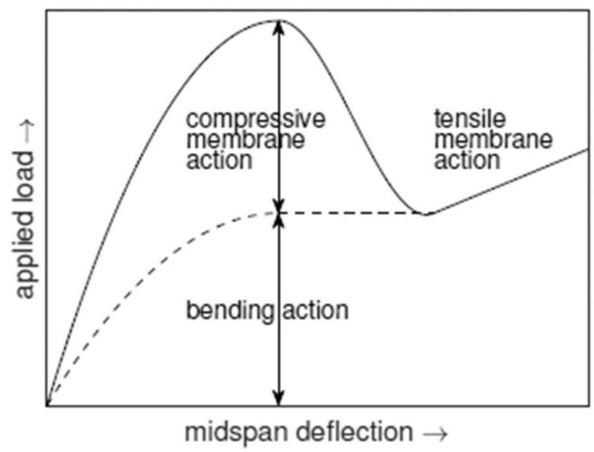

Figure 2. Load-deflection relationship for restrained reinforced concrete slabs, including the effects of membrane action. (Ensink, 2024).

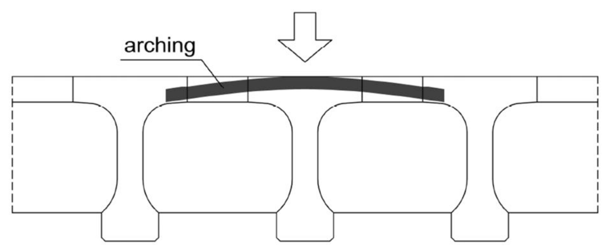

Figure 3. Compressive membrane action for case with load applied at the girder (Ensink, 2024).

2.2.2. Compressive membrane action

Compressive membrane action occurs in restraint slabs as a result of the change in position of the neutral axis, through which an internal arch develops (Hewitt & de Batchelor, 1975, see Figure 2). The results of this mechanism are an increase in the flexural capacity, as well as the punching capacity, which becomes governing (Taylor et al., 2003; 2007; Tong & de Batchelor, 1972). Compressive membrane action is a function of the degree of edge restraint, the member slenderness, and the concrete compressive strength Figure 2.

Previous research on the compressive membrane action in slab-between-girder bridges focused on cases with the load on the slab (Amir et al., 2016). This work showed a linear relation between the transverse post-tensioning force and the punching load. However, the question whether compressive membrane action occurs when the load is placed on top of the girder, see Figure 3, and can activate the adjacent slab portions, has not been addressed experimentally before. For this compressive membrane action to develop, one of the main conditions related to cracking in the cross-section may not be met, as cracking is largely prevented by the presence of the girder. Moreover, a relative deflection between the loading point and arch ends is required to achieve the development of the arching effect. This deflection is restrained by the high stiffness of the girder, and it may be further prevented at loading positions close to the crossbeam. On the other hand, the structural system is expected to create a high horizontal restraint on the sections.

2.2.3. Compressive arching action

In the longitudinal direction in girders, compressive arching action can develop. In essence, arching action in beams results from the basic relation between flexure and shear:

$$V = \frac{d(Tz)}{dx} = \frac{d(T)}{dx}z + \frac{d(z)}{dx}T \tag{2}$$

Where V is the sectional shear, Tz the bending moment expressed as the multiplication of the tension T in the reinforcement and the internal lever arm z. As the lever

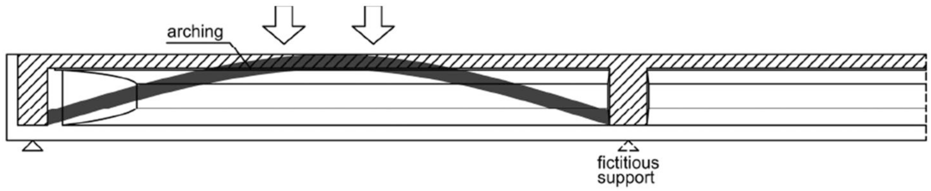

Figure 4. Compressive arching action in girders (Ensink, 2024).

Table 2. Results of initial assessment calculations to determine maximum concentrated live load.

Scenario	x [m]	A [m]	Failure mode	F_{max} [kN]	Relative load capacity [%]
Individual girder	3.4	3.4	flexure-shear	703	106
Individual girder	12.0	12.0	bending moment	662	100
Girder 1 (15) in system	3.8	4.2	shear-tension	1067	161
Girder 1 (15) in system	9.0	9.4	flexure-shear	995	150
Girder 5 (11) in system	1.4	1.8	shear-tension	1652	250
Girder 5 (11) in system	8.4	8.8	shear-tension	1416	214
Girder 8 in system	1.4	1.8	shear-tension	1659	251
Girder 8 in system	8.4	8.8	shear-tension	1424	215

arm decreases towards the support, the portion of arching action can be expressed, whereas the first term is considered the portion of beam action in shear (Alexander, 1990). Arching action has been extensively studied in reinforced concrete beams, often to address shear-compression capacities (Abbasnia & Nav, 2016; Pastore & Vollum, 2022; Reissen et al., 2018). In recent years, similar models of compressive arching action have been developed for prestressed concrete (Gleich & Maurer, 2017; Kiziltan, 2012; Kolodziejczyk & Maurer, 2017). The more advanced models also include an additional compressive axial force resulting from shear. These models help quantify the local arching action in areas close to the supports, resulting in an increase in shear resistance (Huber et al., 2018).

For the girders in slab-between-girder bridges with crossbeams, Figure 4 shows the hypothesised arching effect in the girder. Here, the compressive arching action develops between the first support and the crossbeam, which acts as a fictitious support thanks to the large stiffness of the post-tensioned crossbeam. The same arching action is expected to occur in the girder portion between two crossbeams. This case of arching action differs from the previously researched cases, which mostly considered individual girders, where no hogging moments occur.

2.2.4. Effect of crossbeams

The effect of crossbeams has been studied only to a limited extent. Cai et al. (2002) found that the live load distribution is significantly more beneficial when diaphragms are presented, and that including the stiffness of the diaphragms in finite element models reduces the maximum girder strains. However, the value of the diaphragms stiffness is difficult to estimate. Prestressed diaphragms are expected to be even stiffer, resulting in better load distribution. Moreover, as shown in Figure 4, diaphragms act as intermediate supports in the girder, reducing the bending moment in the longitudinal direction and distributing load in the transverse direction at these points. At the same time, the presence of the crossbeams results in sectional forces being distributed in the system, including the internally developed arching forces, so that a complete arch cannot be achieved.

3. Overview of slab-between-girder bridges in the Netherlands

Between 1953 and 1977, about 70 slab-between-girder bridges were constructed in the Netherlands, and many of these structures are still in use nowadays. As the method is labour-intensive and time-consuming, the construction method is not economically feasible anymore. The existing bridges are often approach bridges for larger main spans over rivers, and often located in the highway network of the country. Typically, these bridges have multiple spans of equal length and are simply supported structures with expansion joints at the piers and abutments. Most bridges are straight or with a negligible skew angle. Table 2 gives an overview of typical dimensions of the bridges. The bridges indicated with an * are not in use anymore. The Vecht Bridge (Vechtbrug) is the topic of this study, and girders from the Helperzoom bridge were tested in the laboratory (Lantsoght et al., 2021; Park et al., 2021; Mustafa et al., 2022; Zhang et al., 2020).

Table 2 shows that the span lengths range between 17 m and 50 m, with an average slenderness of 19.0. The slenderness is related to the girder spacing; with a larger girder spacing resulting in a lower slenderness. Moreover, the girder spacing is related to the girder height. As the width of the top flange increases, the girder spacing increases. Finally, the girder height is also related to the span length. In addition, the number of crossbeams per span, spacing between the crossbeams (at the support to intermediate, and intermediate to intermediate) and width of the crossbeams is also compiled in Supplementary Table A1. The properties of the slab, including the width and thickness of the slab and spacing between girders is also collected in Supplementary Table A1. The thickness of the slabs is relatively constant and ranges between 180 mm and 250 mm. However, as the girder spacing increases, the width of the

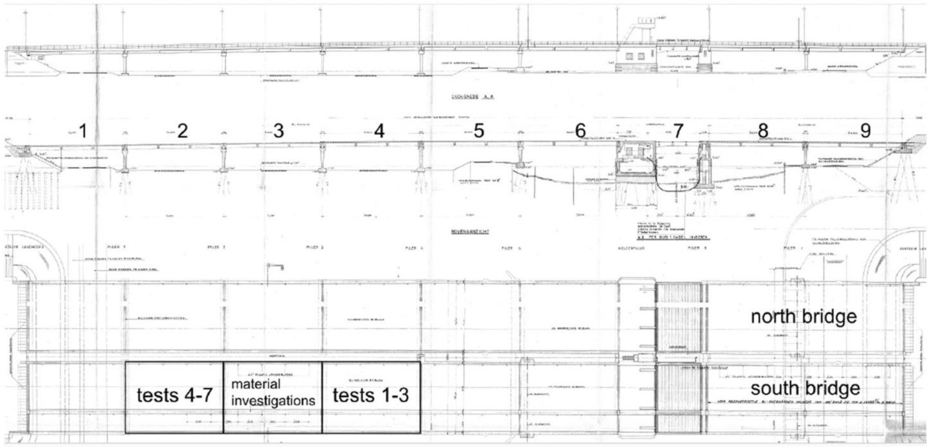

Figure 5. Partial overview of Vecht Bridge, longitudinal section (top) and top view (bottom) (Ensink et al., 2024).

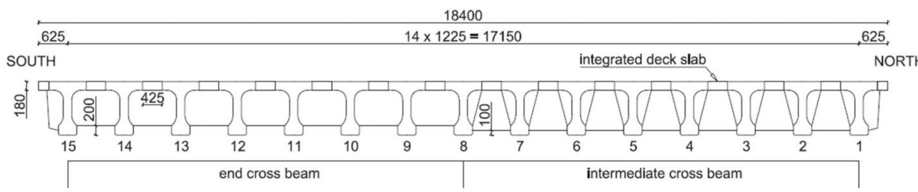

Figure 6. Cross-section of Vecht Bridge with 15 bulb-T girders (measurements in cm) (Ensink, 2024).

slab will increase accordingly, and the slab width ranges from 150 mm to 2780 mm.

4. Description and assessment of Vecht Bridge

4.1. Location and geometry

The Vecht Bridge was a slab-between-girder bridge, consisting of post-tensioned bulb-T girders, post-tensioned slabs cast between the top flanges of the girders, and post-tensioned crossbeams. The Vecht Bridge was built in 1962 in the A1 highway, near the town of Muiden in the province of Noord Holland in the Netherlands. The number of spans was nine, and all spans were simply supported. One span contained a movable bridge over the Vecht River. Two parallel bridges, for both driving directions of the highway, were constructed. As the A1 highway was rerouted to improve traffic flow, the Vecht Bridge became obsolete, and a collapse test in two spans prior to its demolition could be carried out.

Figure 5 shows the western approach bridge, marking the tested spans (spans 2 and 4). In addition, span 3 was used to take core samples of the concrete, to determine the concrete material properties. From span 3, samples of the prestressing tendons were also obtained to determine the properties of the prestressing steel. As identified Supplementary Table A1, the Vecht Bridge has spans of 24 m in length, a girder spacing of 1225 mm, and a slab and top flange of 180 mm. In the transverse direction, 15 prestressed girders are used, as well as crossbeams spaced at 8 m, see Figure 6. The girders were prefabricated on-site and pretensioned after which the ducts were grouted.

Each girder is supported on an individual elastomeric bearing of 206 mm × 306 mm × 46 mm. The bearings are reinforced with three 3 mm thick layers of steel. The outer layers of the bearings consist of synthetic rubber and the two inner layers of 15.5 mm thickness consist of natural rubber. During the 54 years of service life of the bridge, the bearings were never replaced.

4.2. Material properties

Span 3 was used to obtain a large number of samples from the concrete, the reinforcing steel and the prestressing steel (den Boef, 2016; Koekkoek, 2017). A total of 61 concrete cores were taken from the bulb-T girders (top flange, web, and bottom flange, 30 cores in total), the slab (23 cores) and the curb (8 cores). The concrete compressive strength is processed according to the Dutch Guidelines for core testing (Rijkswaterstaat, 2014), including the correction for the core size. On average the cube concrete compressive strength, $f_{cm,cube}$, of the T-girders is found as 106.9 MPa, of the slab 73.5 MPa and of the curb 67.6 MPa. Using a factor of 0.82 to translate to an average cylinder compressive strength $f_{cm,cyl}$ (Gijsbers et al., 2011) gives $f_{cm,cyl} = 87.7$ MPa for the T-girders, 60.3 MPa for the slab, and 55.4 MPa for the curb. On the original drawings, the characteristic cube compressive strength $f_{ck,cube} = 50$ MPa is indicated, which results in an average estimated cylinder compressive strength of $f_{cm,cyl} = 64$ MPa. As such, it can be concluded that the concrete compressive strength has increased over time. Visual inspection of the cores indicated that in general the concrete is well compacted and no signs of deterioration, cracking or reinforcement corrosion are observed. In 7 cores, local poor compaction was observed and in 27 cores, flint aggregates, which could result in alkali-silica reaction, were observed.

The maximum aggregate size was found to range between 26 mm–59 mm.

To determine the material properties of the mild and prestressing steel, three reinforcement bars and four prestressing wires were tested in the laboratory. Of the reinforcement steel, the average yield strength was found to be 287.7 MPa, the average ultimate strength 351.8 MPa and the strain at ultimate 10.0%. This result indicates that reinforcement grade QR24 was used. Of the prestressing steel, the average yield strength was found to be 1505.4 MPa, the average tensile strength 1769.5 MPa and the strain at ultimate 9.0%. This result indicates that prestressing steel grade QP170 was used.

4.3. Reinforcement layout and prestressing forces

In the girders, seven 12ø7 mm ($A_p = 462\,\text{mm}^2$) draped tendons of prestressing steel per girder with 42 mm ducts are provided. The tendons are numbered from 1 through 7, indicating the original order of post-tensioning. The first six tendons are anchored in the anchor block and the 7$^{\text{th}}$ tendon is anchored in the top flange, see Figure 8. Figure 7 shows the layout of the mild steel reinforcement. The reinforcement in the bottom flange of the girders consists of 3ø10 mm bars at 1107 mm from the face of the top flange and 2ø10 mm bars at 980 mm. In the web, 2ø10 mm are provided at 785, 560 and 300 mm. The shear reinforcement consists of ø8 mm stirrups spaced at 500 mm on centre.

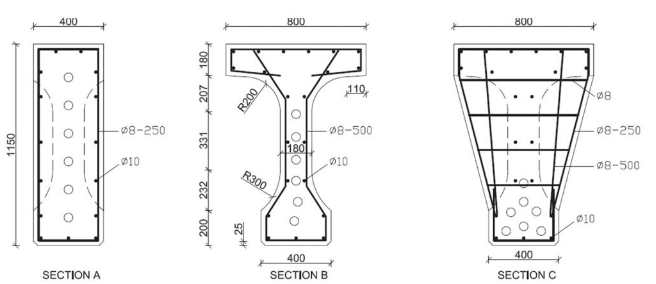

Figure 7. Cross-section of girder at anchorage block (section a), of girder (section B, showing reinforcement details) and at cross-beam (section C). Sections as indicated in Figure 8. Dimensions in mm. (Ensink et al., 2024).

This low amount of shear reinforcement does not fulfil the requirements for minimum shear reinforcement in the current Eurocode. Moreover, the shape of the stirrups follows the shape of the girder, which is not permitted anymore nowadays.

The transverse post-tensioning in the slab and diaphragms consists of 12ø7 mm ($A_p = 462\,\text{mm}^2$) per tendon in ducts of ø50 mm, with a total of 59 transverse post-tensioning tendons per span. In the slab, 35 unevenly spaced post-tensioning tendons are provided. The tendons are more closely spaced in the vicinity of the intermediate crossbeams. In the intermediate crossbeams, eight straight tendons are provided and in the end crossbeams five post-tensioning tendons are provided, two of which are provided in the top flange. With the exception of the transverse post-tensioning, there is no steel reinforcement connecting the cast in-between slab to the girder. The concrete surface is roughened at the T-girder to improve the connection to the slab. In the slab, the mild reinforcement consists of 4ø6 mm bars and stirrups ø6 mm at 400 mm on centre. In the crossbeams, the mild steel reinforcement consist of 5 ø8mm bars top and bottom and stirrups of ø8 mm at 200 mm on centre.

4.4. Initial assessment using linear finite element analysis

To prepare for the collapse test, an extensive initial assessment using linear finite element analysis is carried out, with the aim of determining the maximum concentrated load during the test and the critical location and to frame the experiments in the methods used for assessment of existing bridges in the Netherlands. For this purpose, the first step is thus to carry out an assessment of the bridge using linear finite element analysis, modified to the use of a single concentrated load to mimic the test procedures. The analysis considers all possible load positions along the length of the girder, indicated as positions a_i. Then, for every load position a_i all control sections x_j are evaluated for cracking moment, shear-tension, flexure-shear, and bending moment. To be able to compare the different failure mechanisms, load factors are used. The procedure determines the overall

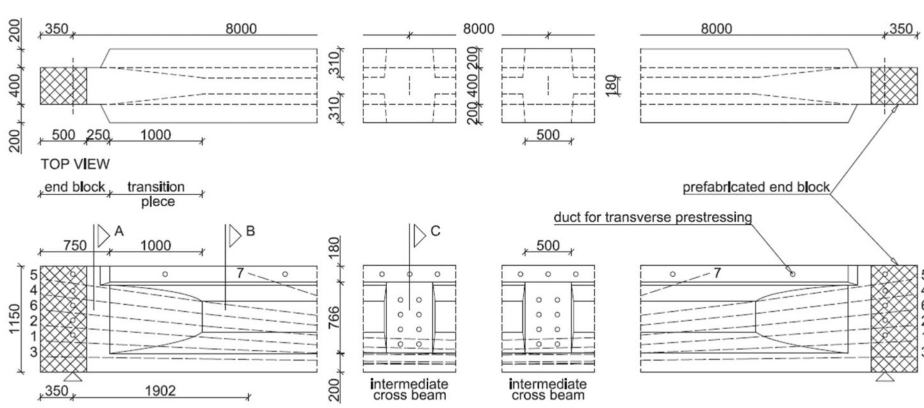

Figure 8. Detail of draped tendon layout in T-girder (dimensions in mm) (Ensink et al., 2024).

governing load factor, which provides information on the governing failure mechanisms, critical load position, and critical section. Figure 9 summarises the procedure used to determine the governing load factor. Figure 10 shows the results as a function of the control section for girder 5 in the system, indicating that shear is governing over flexure. No results are provided near the crossbeam as the cross-beams acts as an interior support.

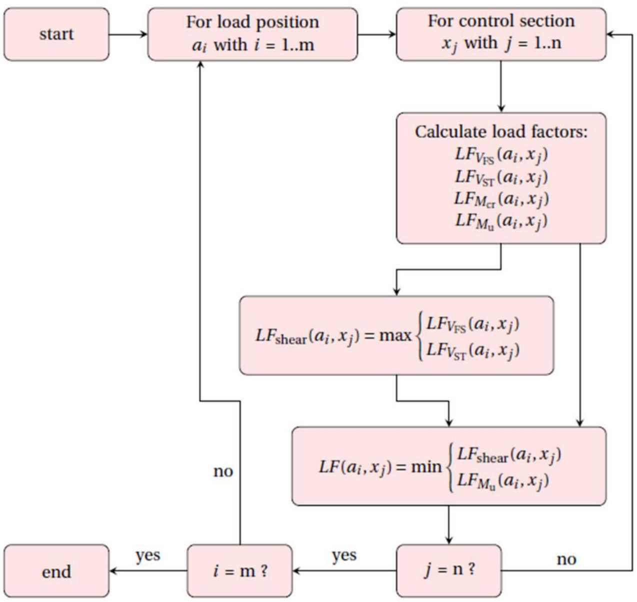

Figure 9. Flowchart of procedure for assessment calculation (Ensink, 2024).

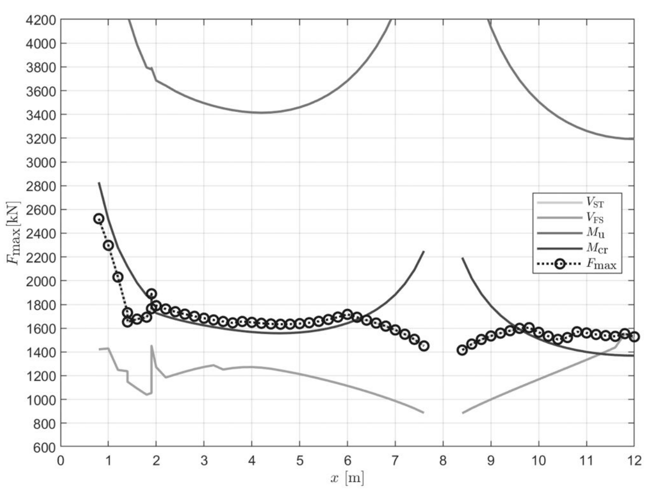

Figure 10. Maximum load for all critical sections, illustrating results of girder 5 (11) (Ensink, 2024).

Table 2 gives an overview of the results of the assessment calculations. The relative load capacity compares the maximum load of the calculation to the case of the individual girder failing in flexure at 662 kN. As the cross-section is symmetrical, the results for girders 1 and 15 are the same, and the results for girders 5 and 11 are the same. Girder 8 is placed in the middle of the transverse section. The results show that the governing failure mode for the majority of cases is shear-tension. For the girders in the system, the governing control section is not close to the support, but near the intermediate cross-beam. The exterior girder (girder 1 and 15) is more sensitive to flexure-shear than the interior girders. Flexure does not govern at any location for the girders in the system, and the ratio between the maximum load for flexure and maximum calculate load is more than 2 for the critical positions. The girder in the system has a maximum load between 1.5–2.5 times the maximum load on the individual girder.

5. Test setup

5.1. Load positions

The experiments on the Vecht Bridge were done in October 2016. The connected system in span 4 was used for three experiments (of which two were continued to failure), and the span with saw cuts, span 2 (Figure 11), was used for four experiments. Figure 5 and Table 3 summarise the experimental findings. In span 4, the original structural system is unaltered. Tests 1 and 2 aim at testing interior girders and quantifying the effect of load distribution and redistribution, and at least four girders are present between the tested girder and the edge. In test 3, the exterior girder itself is tested. Test 3 is stopped at 250 tons, as this load was identified as the maximum load for stability of the applied loading system. The saw cut in span 2 cuts through the slabs and three out of the four crossbeams. The cross-beam on the opposite side is not sawn. By comparing the

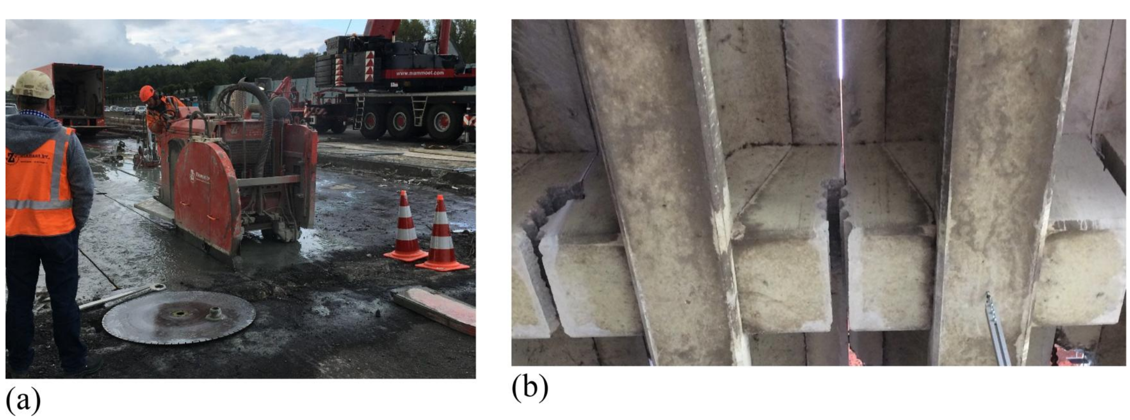

Figure 11. Photographs of sawing the slab and crossbeams (Ensink, 2024): (a) sawing through the deck slab; (b) sawing and drilling through the diaphragm.

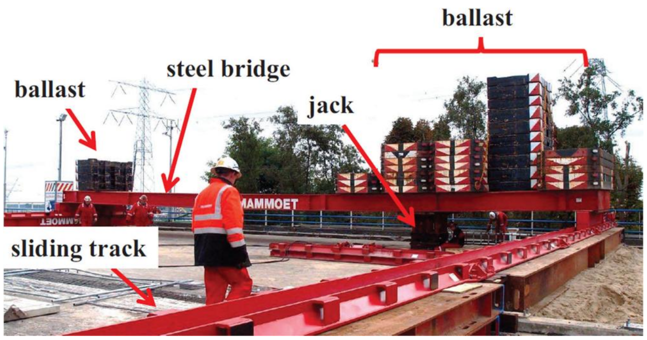

Figure 12. Load application system (Ensink, 2024).

test results of the full structural system in span 4 to the individual girder behaviour in span 2, the effects of the system behaviour can be quantified.

The load position in the experiments is selected based on an initial calculation. The results in Table 2, which were carried out later to mimic a full assessment procedure, are a refinement of the initial calculations used to prepare for the experiments. Therefore, load positions of 4000 mm (in the middle of the 'span' between the end and intermediate crossbeams, to study the effect of arching), and 2250 mm (first estimate of the flexure-shear critical position because of the prestressing tendon layouts) are selected for the experiments. Moreover, the same loading position is used in spans 2 and 4, to have a direct comparison between the isolated girders and the girders in the system.

5.2. Loading system

The single concentrated load is applied using a loading plate of 400 mm × 400 mm and by using a hydraulic jack of 6000 kN with a stroke of 250 mm. Figure 12 shows the full loading system, built up using a 25 m steel spreader beam of 24.3 m with counterweights (ballast) on top. When the system is not activated, the load flows to the supports. When the system is activated, the load is gradually applied from the steel spreader beam to the girder *via* the jack. The capacity of the system applied in this experiment is approximately 4000 kN. This system has been used in the Netherlands in a previous collapse test (Lantsoght et al., 2017c) and in proof load tests in viaducts Zijlweg (Lantsoght et al., 2017a) and de Beek (Lantsoght et al., 2017b). To facilitate the larger number of test on the bridge, a sliding system was added to the original design of the loading system as used previously; this element is identified as 'sliding track' in Figure 12. The sliding track contained a jack to move the spreader beam and was equipped with Teflon blocks to facilitate the sliding.

For the girder tests in span 2, steel chains were provided through drilled holes in the slab. These chains were anchored to an additional steel beams (a static and dynamic beam), designed to take the static and dynamic forces in case the girder should collapse completely and fall into the chains. This measure was carried out for safety reasons to avoid that the failed beam would fall in the ground under the bridge.

Table 3. Overview of tests on the Vecht bridge.

Test	Span	Distance from support [mm]	Structural system	Type of test
1	4	4000	not changed	Interior girder
2	4	2250	not changed	Interior girder
3	4	2250	not changed	Exterior girder
4	2	2250	saw cut	Individual girder
5	2	2250	saw cut	Individual girder
6	2	2250	saw cut	Individual girder
7	2	4000	saw cut	Individual girder

5.3. Instrumentation

To reduce the time on site, the instrumentation on the experiments is kept to a minimum. Linear potentiometers are used to measure the deflections. The applied load at the hydraulic jack is measured using a load cell. The vertical deformation of the girders and at the crossbeam are measured using linear potentiometers installed on aluminium frames from the ground under the bridge. The deformations at the bearings are measured using a potentiometer next to the bearings. The relative vertical slab deformation is measured using linear potentiometers on both sides of the tested girder. An LVDT over 1 m is also used to measure smeared strains. Figure 13 gives an example of the instrumentation plan used in the first test.

6. Test results

6.1. Failure loads

The results of the experiments are summarised in Table 4, including the test number and span, with experiments in span 4 on the system and in span 2 on the girders after applying the saw cuts. The value of a/d is the ratio of the shear span a (as given in Table 3) to the effective depth d of the girder. F_{max} is the failure load in the test and δ_u is the maximum deflection. The sectional shear at failure V_R is calculated by considering the dead load, the prestressing force, and the externally applied load (F_{max} at failure).

Table 4 also describes the failure mode observed in the experiments. For tests 1 and 2, Figure 14 shows the shear failure in the girder and Figure 15 shows the punching failure in the deck, where the failure initiated. All experiments on the individual girders resulted in a flexural shear failure, as exemplified in Figure 16. In experiments 4 through 6, the unreinforced concrete filling at the anchorage location of tendon 7 burst out. Figure 17 gives the load-deflection diagram of the experiments in span 4 and Figure 18 gives this result of the experiments in span 2.

From the test results, it can be observed that all individual tests resulted in a flexure-shear failure of the girder. The scatter between tests 4 through 6, all carried out with the same loading position is only 6%. Test 7 gives a low maximum load of only 59% of the load in experiments 4 through 6.

6.2. Comparison of individual girders and system

A first analysis looks at comparing the results from span 4 (system behaviour) to span 2 (saw cut). Figure 19 contains

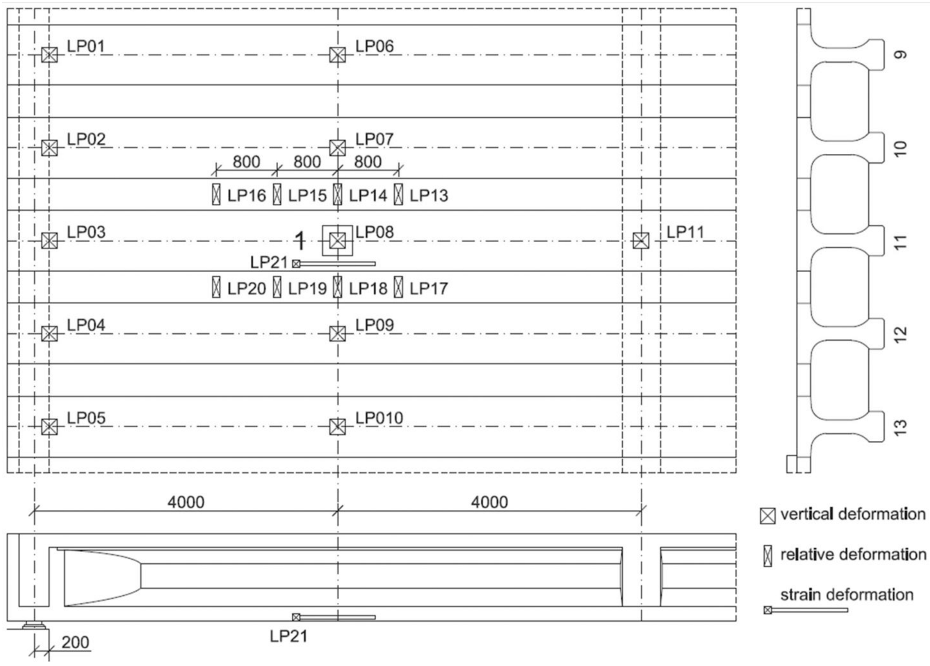

Figure 13. Instrumentation for test 1 (dimensions in mm) (Ensink, 2024).

Table 4. Summary of experimental results.

Test	Span	a/d	F_{max} [kN]	V_R [kN]	δ_u [mm]	Failure mode
1	4	4.8	3004	1188	21	Punching of deck and shear failure of girder
2	4	2.8	3444	1525	14	Punching of deck and shear failure of girder
3	4	2.8	2506	998	11	Not tested to failure
4	2	2.8	1678	1301	79	Flexural shear T-girder
5	2	2.8	1703	1323	65	Flexural shear T-girder
6	2	2.8	1774	1385	74	Flexural shear T-girder
7	2	4.8	1022	774	132	Flexural shear T-girder

Figure 14. Shear failure of T-girder in test 1. The crossbeam is located on the left side and the end support on the right side (Ensink et al., 2024).

this comparison based on the results of the sectional shear at failure, indicating that the sectional shear at failure is larger in the system than in the individual member. For $a/d = 2.8$, the system is 114% of the individual shear and for $a/d = 4.8$ this value is 153%. However, a number of aspects play a role here, including load distribution and redistribution, which result in a change of failure mode from flexure-shear in the individual girders to punching and shear-tension in the system. In the system, compressive membrane action in the slab and compressive arching action in the beam provide additional capacity. The cross-beams also increase the capacity, as the crossbeams work as an internal support.

Using the shear distribution factor for interior girders from AASHTO (see Equation (1)), a factor of 0.52 is found. For $a/d = 2.8$, the maximum load in span 4 is 3444 kN, which corresponds to a maximum load on the tested girder of 1791 kN according to this distribution factor. This value can be compared to the average maximum load of the three experiments in span 2 with $a/d = 2.8$ of 1718 kN, which is slightly lower. For $a/d = 4.8$ the maximum load in the connected system is 3004 kN, which would give a maximum load on the tested girder of 1562 kN. The failure load in test 7 was 1022 kN. This brief comparison shows that the AASHTO distribution factors cannot fully capture the complex system behaviour at the ultimate limit state and different shear failure mechanisms that occur in the system.

7. Discussion

As shown in the literature review, collapse tests on bridges are a rare type of experiment, difficult to prepare, and

(a) (b)

Figure 15. Punching failure of the deck slab in test 1: (a) top view and measurements in cm; (b) bottom view (right) (Ensink et al., 2024).

Figure 16. Flexural shear failures in test 4 and 5 (Ensink et al., 2024).

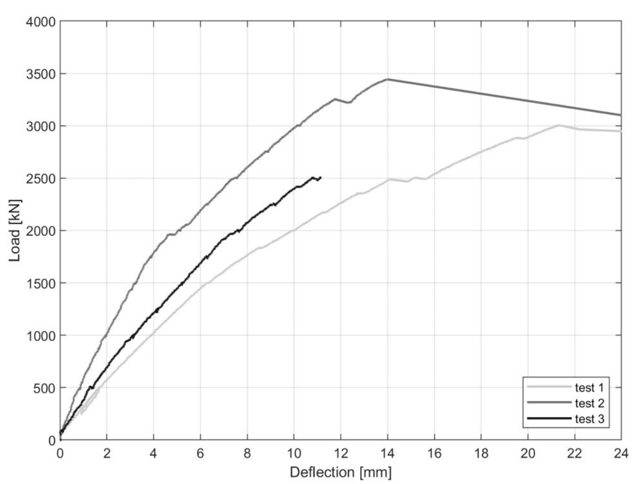

Figure 17. Load-deflection diagrams of girders in span 4 (Ensink et al., 2024).

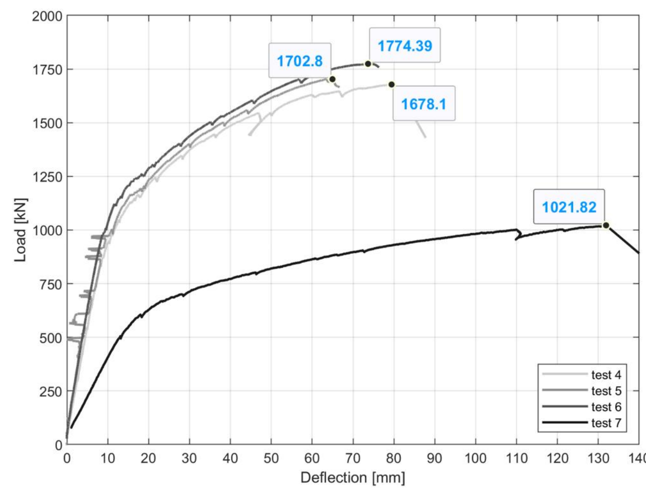

Figure 18. Load-deflection diagrams of girders in span 2 (Ensink et al., 2024).

sometimes resulting in unexpected outcomes. The presented experiments on the Vecht Bridge are unique for a number of reasons: 1) the structural system tested, 2) the careful preparation to obtain the intended shear failure during the experiments, and 3) the ability to compare between the behaviour in the full structural system and the girders obtained after a saw cut through the deck.

To compare the behaviour of the individual girder to the girder in the system, we have analysed both the sectional shear (which, in itself is influenced by load distribution in the system) and the maximum load at failure. The experimental results are compared to the AASHTO load distribution factor and to the expected load distribution obtained with a linear finite element analysis. It is expected from the linear finite element analysis that the total load on the system is between 2 and 2.5 times larger than the load on the individual girder (see Table 2), and similarly, the AASHTO load distribution factor is 0.52, meaning that 0.52 times the applied load is carried by the tested girder. The test results show a larger effect of the system behaviour for the experiments with a larger distance between the load and the support ($a/d = 4.8$) as compared to those with the load closer to the support ($a/d = 2.8$). The sectional shear in the system is on average 114% that of the individual girder for $a/d = 2.8$ and 153% for $a/d = 4.8$, and the maximum load is on average 200% for the system as compared to the individual girder for $a/d = 2.8$ and 294% for $a/d = 4.8$. Overall, the load distribution found in the linear finite element model is in line with the experimental observations, and slightly on the conservative side. Finally, we can also observe that the overall system is much stiffer (as evidenced by the smaller deflections at the ultimate) than the individual girders: the deflection of the system at ultimate is 19% of the deflection of the individual girder for $a/d = 2.8$ and 16% for $a/d = 4.8$.

However, comparing the expected failure loads with the experimentally observed loads, show a larger maximum load

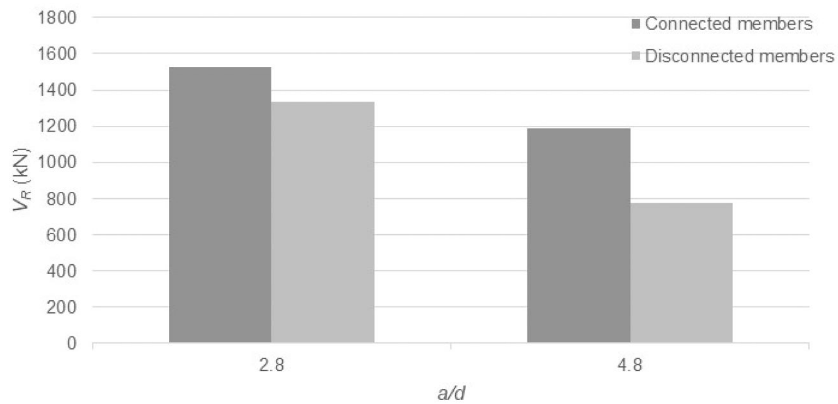

Figure 19. Comparison between sectional shear force at failure for connected and disconnected members from Table 4. Note that the average result of tests 4–6 is used for this comparison.

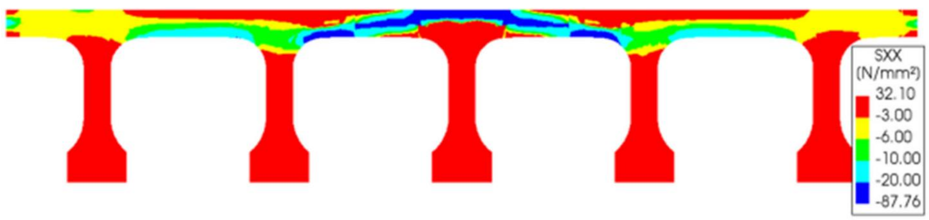

Figure 20. Nonlinear finite element model, identifying development of compressive membrane action (Ensink, 2024).

for both the individual girders and the girders in the system. For the individual girders, this observation can be attributed to the compressive arching action that develops in the beam to a certain extent. The larger increase in capacity for the elements in the system shows the contribution of additional load-carrying mechanisms, such as compressive membrane action in the deck, compressive arching action in the girder, and the restraint and intermediate support as provided by the crossbeams. The reader should note here that compressive membrane action occurred in these experiments, even though the load was placed about the girder. This insight is further supported by the insights gathered from the nonlinear finite element analysis which is carried out as part of the research, but outside of the scope of the current paper, see Figure 20. The mechanism stipulated in Figure 3 is thus observed experimentally and confirmed through numerical analysis. In other words, we have provided the first experiments showing that compressive membrane action can also be activated when the load is not in the middle of the deck, but right on top of the girder.

Moreover, the bridge system failed through punching of the deck above the girder. If such a punching failure can be avoided (as expected for a tandem with four wheel prints in comparison to the single wheel print used in the experiments), it is expected that the maximum load on the system can be further increased and the premature punching failure can be avoided. The observation on the large difference between overall system behaviour in bridges and the capacity of individual elements aligns with observations made earlier in the literature to align system behaviour into bridge design (Ghosn & Moses, 1998; Miao & Ghosn, 2016). The two compressive mechanisms should be analysed together, and both depend on the restraint provided by the overall system to anchor the line of thrust of the arches. The result of this global bridge behaviour is that the force flow and failure mechanism differs in the bridge system as compared to the individual girders, which all failed in flexure-shear.

While collapse testing of bridges is expensive (order of magnitude of 400 k€), the cost savings for the service life extension of the other slab-between-girder bridges (where replacement would cost over 10 m€) is significant (approximately 45% cost savings on a 100-year time horizon when comparing annual equivalent costs). Moreover, indirect cost savings from avoiding traffic delays and ecological cost savings related to material use and transportation are obtained, and these indirect cost savings could be quantified in a societal cost-benefit analysis. Based on previous projects, it is expected that these indirect cost savings will be even larger than the direct cost savings (Hendy & Petty, 2012).

At this moment, the effect of compressive membrane action and compressive arching action is studied only for the case of the Vecht Bridge. Besides the experimental work, extensive nonlinear finite element models have been used to study the force flow in the bridge in detail (Ensink, 2024), looking both at the overall structure, a girder with the boundary conditions as in the bridge, and a fully isolated girder. A next step would be the extension to the geometries of the existing slab-between-girder bridges in the Netherlands, so that the insights can be broadly applied to the assessment of these bridge types.

8. Conclusions

This paper reviews the existing literature regarding collapse testing, global bridge behaviour (both topics as applicable to prestressed slab-between-girder bridges in the Netherlands), gives an overview of typical geometries of these bridges in the Netherlands, reports the results of seven experiments of collapse testing the Vecht Bridge, and analyses the difference between the capacity of the individual girders and the girders in the system. The Vecht Bridge was a slab-between-girder bridge, consisting of 15 post-tensioned girders in the cross-section, concrete slabs cast between the top flanges of the girders and post-tensioned transversally, and four post-tensioned crossbeams (at the ends and at one third of the span). As such, the Vecht Bridge is an excellent case to study global bridge behaviour, and this analysis was facilitated by testing the global bridge behaviour in one span (span 4, three experiments) and providing a saw cut through the deck and crossbeams for testing the individual girders in another span (span 2, four experiments).

From the literature review and discussed experiments, we can draw the following conclusions:

- Collapse testing is only carried out in exceptional cases, requires careful preparation and execution, and gives unique insights.
- The seven experiments carried out on the Vecht Bridge resulted in the expected shear failure. The shear failure mode differs between the system (punching in the deck combined with shear-tension in the girder) and the individual girder (flexure-shear failure).
- Linear finite element analysis and the AASHTO distribution factors give an overall estimation of the load distribution in the system, but the capacity of the individual girders and the connected girders are larger than estimated using code equations as a result of the additional load-carrying mechanisms that occur.
- In particular, for the failure load in the system, the maximum load is significantly larger than expected as the result of the combination of compressive membrane action in the deck and compressive arching action in the girder, as well as the effect of the presence of the crossbeams.

In conclusion, the experiments on the Vecht Bridge give us a unique insight into the behaviour and ultimate capacity of a real slab-between-girder bridge that has been in service for decades, and that contains all the original details.

List of Notations

a	shear span, distance from the centre of the load to the centre of the support
a_i	possible load positions
d	effective depth
$f_{ck,cube}$	characteristic cube compressive strength of the concrete
$f_{cm,cube}$	average cube compressive strength of the concrete
$f_{cm,cyl}$	average cylinder compressive strength of the concrete
x_j	analysed sections
z	internal lever arm
DF	distribution factor
ECB	exterior crossbeam
F	flexural failure
F_{max}	maximum load
HJ	load applied using hydraulic jack
ICB	interior crossbeam
LF	load factor, used in the linear finite element analysis
M_{cr}	cracking moment
M_u	ultimate moment
P	punching failure
S	shear failure
S	girder spacing in ft
T	tension in reinforcement bar
V	sectional shear
V_{FS}	sectional shear at flexure-shear failure
V_R	sectional shear at failure in the experiments
V_{ST}	sectional shear at shear-tension failure
W	load applied using kentledge weight
δ_u	maximum deflection

Acknowledgements

The authors wish to express their gratitude and sincere appreciation to the Dutch Ministry of Infrastructure and Water Management (Rijkswaterstaat) for financing this research work. The contributions and help of our (former) colleagues Dick Hordijk, Rutger Koekkoek, Marco Roosen, Fred Schilperoort, Cor van der Veen, and Yuguang Yang, and of student Thomas Harrewijn of Delft University of Technology are gratefully acknowledged. The fruitful discussions with Ane de Boer, Sonja Fennis, and Herbert van der Ham from the Dutch Ministry of Infrastructure and Water Management, with Frank Linthorst and Danny den Boef of Witteveen + Bos, responsible for logistics and safety during the test, and with Otto Illing and the late Chris Huissen of Mammoet, responsible for applying the load during the collapse test, are also acknowledged.

Author contributions

CRediT: **Sebastiaan W. H. Ensink**: Formal analysis, Investigation, Methodology, Writing – review & editing; **Eva O. L. Lantsoght**: Conceptualization, Investigation, Methodology, Project administration, Supervision, Writing – original draft; **Max A. H. Hendriks**: Supervision, Writing – review & editing.

Disclosure statement

No potential conflict of interest was reported by the author(s).

Funding

This research received funding from the Dutch Ministry of Infrastructure and Water Management (Rijkswaterstaat).

ORCID

Eva O. L. Lantsoght http://orcid.org/0000-0003-4548-7644

Data availability statement

The data is available upon request.

References

AASHTO. (2015). *AASHTO LRFD bridge design specifications, 7th edition with 2015 interim specifications* (7th ed.). American Association of State Highway and Transportation Officials.

Abbasnia, R., & Nav, F. M. (2016). A theoretical method for calculating the compressive arch capacity of RC beams against progressive collapse. *Structural Concrete*, *17*(1), 21–31. https://doi.org/10.1002/suco.201400119

ACI Committee 342. (2016). *ACI 342R-16: Report on Flexural Live Load Distribution Methods for Evaluating Exisiting Bridges* (p. 36). American Concrete Institute.

Alampalli, S., Frangopol, D. M., Grimson, J., Halling, M. W., Kosnik, D. E., Lantsoght, E. O. L., Yang, D., & Zhou, Y. E. (2021). Bridge load testing: State-of-the-practice. *Journal of Bridge Engineering*, *26*(3), 03120002. https://doi.org/10.1061/(ASCE)BE.1943-5592.0001678

Alexander, S. D. B. (1990). *Bond model for strength of slab-column joints* [PhD Thesis]. University of Alberta.

Amir, S. (2014). *Compressive membrane action in prestressed concrete deck slabs* [Ph.D. Thesis]. (pp. 317). Delft University of Technology.

Amir, S., Van der Veen, C., Walraven, J. C., & de Boer, A. (2016). Experiments on punching shear behavior of prestressed concrete bridge decks. *ACI Structural Journal*, *113*(3), 627–636.

Arockiasamy, M., & Amer, A. (1998). Load distribution on highway bridges based on field test data. *Phase*, *III*, 170.

Bagge, N., Popescu, C., & Elfgren, L. (2018). Failure tests on concrete bridges: Have we learnt the lessons? *Structure and Infrastructure Engineering*, *14*(3), 292–319. https://doi.org/10.1080/15732479.2017.1350985

Bareš, R., Massonnet, C. E., & Vaněk, J. (1968). *Analysis of beam grids and orthotropic plates by the Guyon-Massonnet-Bareš method.*

Benítez, J. M. P., Benjumea, J. M., & Haach, V. G. (2022). Theoretical and computational simulation of the effect of the number of intermediate diaphragms on the live load distribution factors and structural response of a precast girder bridge. *Latin American Journal of Solids and Structures*, *19*(5), 1–14. https://doi.org/10.1590/1679-78257120

Cai, C. S., Shahawy, M., & Peterman, R. J. (2002). Effect of diaphragms on load distribution of prestressed concrete bridges. *Transportation Research Record, 1814(Design of Structures)*, *1814*(1), 47–54. https://doi.org/10.3141/1814-06

CEN. (2003). *Eurocode 1: Actions on structures - Part 2: Traffic loads on bridges, NEN-EN 1991-2:2003* (pp. 168).

CEN. (2005). (2005). Eurocode 2: Design of concrete structures - part 1-1 general rules and rules for buildings. NEN-EN. 1992-1-1 Comité Européen de Normalisation (pp. 229).

den Boef, D. (2016). Proefbelasting KW "Vechtbrug A1" - Materiaalkundig onderzoek betondruksterkte. Deventer, The Netherlands (pp. 79).

Dutch Institute for Normalization. (1962). *NEN 1009:1962 provisions reinforced concrete.*

Ensink, S., Lantsoght, E., & Hendriks, M. (2024). Collapse test of prestressed concrete slab-between-girder bridge. *IABMAS*, *2024*, 289–296.

Ensink, S. W. H. (2024). *System behaviour in prestressed concrete T-beam bridges* [PhD. Thesis]. (pp. 286). Delft University of Technology.

Gijsbers, F. B. J., Steenbergen, R. D. J. M., & van der Veen, C. (2011). *Werkset factoren plaatconstructies van gewpaend beton zonder dwarskrachtwapening*. TNO/TU Delft Report 24.

Ghosn, M., & Moses, F. (1998). Redundancy in highway bridge superstructures NCHRP Report 406. Transportation Research Board.

Gleich, P., & Maurer, R. (2017). Bridge reassessment in Germany: Shear capacity computation based on arch action model. *Proceedings of the Institution of Civil Engineers - Engineering History and Heritage*, *170*(3), 112–124. https://doi.org/10.1680/jenhh.16.00024

Hendy, C., & Petty, R. (2012). Quantification of sustainability principles in bridge projects. In F. Biondini and D. M. Frangopol (Eds.), *Proceedings of the sixth international conference on bridge maintenance, safety and management* (pp. 1793–1800). Taylor & Francis.

Hewitt, B. E., & de Batchelor, B. V. (1975). Punching shear strenght of restrained slabs. *Journal of the Structural Division*, *101*(9), 1837–1853. https://doi.org/10.1061/JSDEAG.0004158

Huber, P., Huber, T., & Kollegger, J. (2018). Influence of loading conditions on the shear capacity of post-tensioned beams with low shear reinforcement ratios. *Engineering Structures*, *170*, 91–102. https://doi.org/10.1016/j.engstruct.2018.05.079

Idriss, R. L., & Liang, Z. (2010). In-service shear and moment girder distribution factors in simple-span prestressed concrete girder bridge - measured with built-in optical fiber sensor system. *Transportation Research Record: Journal of the Transportation Research Board*, *2172*(1), 142–150. https://doi.org/10.3141/2172-16

Jáuregui, D. V., & Barr, P. J. (2004). Nondestructive Evaluation of the i-40 bridge over the Rio Grande River. *Journal of Performance of Constructed Facilities*, *18*(4), 195–204. https://doi.org/10.1061/(ASCE)0887-3828(2004)18:4(195)

Kiziltan, H. (2012). *Zum Einfluss des Druckbogens auf den Schubwiderstand von Spannbetonbalken* [PhD Thesis].

Koekkoek, R. T. (2017). *Measurement Report Loading of Vechtbrug (25H-100). Stevin Report 25.5-17-03* (pp. 55).

Kolodziejczyk, A., & Maurer, R. (2017). Arch action model applied to existing prestressed concrete bridges in Germany. *Proceedings of the Institution of Civil Engineers - Engineering History and Heritage*, *170*(3), 99–111. https://doi.org/10.1680/jenhh.16.00025

Lantsoght, E. O. (2024). Assessment of existing concrete bridges by load testing: Barriers to code implementation and proposed solutions. *Structure and Infrastructure Engineering*, *20*(7-8), 1002–1014. https://doi.org/10.1080/15732479.2023.2264825

Lantsoght, E. O. L., van der Veen, C., Walraven, J. C., & de Boer, A. (2013). Shear Assessment of Reinforced Concrete Slab Bridges. International IABSE Conference, Assessment, Upgrading and Refurbishment of Infrastructures, *8*, 76–77. pphttps://doi.org/10.2749/222137813806474327

Lantsoght, E. O. L., Koekkoek, R. T., Hordijk, D. A., & De Boer, A. (2017a). Towards standardization of proof load testing: Pilot test on viaduct Zijlweg. *Structure and Infrastructure Engineering, pp*, *14*(3), 365–380. https://doi.org/10.1080/15732479.2017.1354032

Lantsoght, E. O. L., Koekkoek, R. T., van der Veen, C., Hordijk, D. A., & de Boer, A. (2017b). Pilot proof-load test on Viaduct De Beek: Case study. *Journal of Bridge Engineering*, *22*(12), 05017014. https://doi.org/10.1061/(ASCE)BE.1943-5592.0001131

Lantsoght, E. O. L., Van der Veen, C., De Boer, A., & Hordijk, D. A. (2017c). Collapse test and moment capacity of the Ruytenschildt Reinforced Concrete Slab Bridge. *Structure and Infrastructure Engineering*, *13*(9), 1130–1145. https://doi.org/10.1080/15732479.2016.1244212

Lantsoght, E. O. L., Koekkoek, R., van der Veen, C., & Sliedrecht, H. (2019a). Fatigue assessment of prestressed concrete slab-between-girder bridges. *Applied Sciences*, *9*(11), 2312. https://doi.org/10.3390/app9112312

Lantsoght, E. O. L., Van der Veen, C., Koekkoek, R. T., & Sliedrecht, H. (2019b). Punching capacity of prestressed concrete bridge decks under fatigue. *ACI Structural Journal*, *116*(4), 209–2018.

Lantsoght, E. O. L., Van der Veen, C., Koekkoek, R. T., & Sliedrecht, H. (2019c). Fatigue testing of transversely prestressed concrete decks. *ACI Structural Journal*, *116*(4), 143–154.

Lantsoght, E. O. L., Zarate, G., Zhang, F., Yang, Y., Park, M., & Sliedrecht, H. (2021). Shear experiments of prestressed concrete bridge girders. *ACI Structural Journal*, *118*(3), 117–130.

Miao, F., & Ghosn, M. (2016). Reliability-based progressive collapse analysis of highway bridges. *Structural Safety*, *63*, 33–46. https://doi.org/10.1016/j.strusafe.2016.05.004

Mordak, A. G., & Manko, Z. (2008). Static Load Tests of Posttensioned, Prestressed Concrete Road Bridge over Reservoir Water Plant. *Transportation Research Record: Journal of the Transportation Research Board*, *2050*(1), 90–97. https://doi.org/10.3141/2050-09

Park, M. K., Lantsoght, E. O. L., Zarate Garnica, G. I., Yang, Y., & Sliedrecht, H. (2021). Analysis of shear capacity of prestressed concrete bridge girders. *ACI Structural Journal*, *118*(6), 75–89. https://doi.org/10.14359/51733000

Pastore, M. V. F., & Vollum, R. L. (2022). Shear enhancement in RC beams without shear reinforcement simultaneously loaded within 2d and at 3d from supports. *Structures*, *42*, 343–366. 2022/08/01/ https://doi.org/10.1016/j.istruc.2022.05.095

Pimentel, M., Figueiras, J., Félix, C., Cavadas, F., Tomé, E., Rodrigues, C., & Costa, B. (2023). *Load Tests on Bridges. Advances on Testing* *and Experimentation in Civil Engineering: Materials, Structures and Buildings* (C. Chastre, J. Neves, D. Ribeiro, M. G. Neves, and P. Faria, Eds., pp. 219–240). Springer International Publishing.

Reissen, K., Classen, M., & Hegger, J. (2018). Shear in reinforced concrete slabs—Experimental investigations in the effective shear width of one-way slabs under concentrated loads and with different degrees of rotational restraint. *Structural Concrete*, *19*(1), 36–48. https://doi.org/10.1002/suco.201700067

Rijkswaterstaat. (2014). *Richtlijnen voor boren, transporteren en beproeven van betonkernen en het bepalen van druk- en splijttreksterkte*. RTD 1018:2014, Rijkswaterstaat, Utrecht, the Netherlands.

Rijkswaterstaat. (2020). *Beeldarchief rijkswaterstaat*.

Saroufim, A., Issa, M. A., Mahdi, M., & Issa, M. A. (2023). Proof load testing and shear assessment of kishwaukee I-39-river bridge using the modified compression field theory. *Journal of Civil Structural Health Monitoring*, *13*(2-3), 827–866. https://doi.org/10.1007/s13349-022-00667-0

Sato, Y., Prayoonwet, W., & Oshima, Y. (2019). Investigation on structural behavior of existing prestressed post-tensioned concrete bridge superstructure. *International Federation for Structural Concrete*, 1021–1028. International Federation for Structural Concrete.

Mustafa, S., Lantsoght, E. O. L., Yang, Y., & Sliedrecht, H. (2022). Numerical analysis of prestressed concrete bridge girders failing in shear. *ACI Structural Journal*, *119*(6), 11–/11. / https://doi.org/10.14359/51736109

Taylor, S. E., Rankin, G. I. B., & Cleland, D. J. (2003). Real strength of high-performance concrete bridge deck slabs. *Proceedings of the Institution of Civil Engineers - Bridge Engineering*, *156*(2), 81–90. https://doi.org/10.1680/bren.2003.156.2.81

Taylor, S. E., Rankin, B., Cleland, D. J., & Kirkpatrick, J. (2007). Serviceability of bridge deck slabs with arching action. *ACI Structural Journal*, *104*(1)), 39–48.

Tong, P. Y., & de Batchelor, B. V. (1972). Compressive membrane enhancement in two-way bridge slabs. *Aci SP*, *30-12*, 271–286.

Wekezer, J., Kwasniewski, L., & Malachowski, J. (2004). *Analytical and experimental evaluation of existing Florida DOT bridges* (pp. 272).

Zhang, F., Zarate Garnica, G. I., Yang, Y., Lantsoght, E., & Sliedrecht, H. (2020). Monitoring shear behavior of prestressed concrete bridge girders using acoustic emission and digital image correlation. *Sensors*, *20*(19), 5622. https://doi.org/10.3390/s20195622